Geophys. J. Int. (2007) **170,** 961–970 doi: 10.1111/j.1365-246X.2007.03442.x

A finite element analysis of tidal deformation of the entire earth with a discontinuous outer layer

H. L. Xing[1,2], J. Zhang[1] and C. Yin[1,2]

[1]*Earth Systems Science Computational Centre (ESSCC), Sir James Foots Building (47a), The University of Queensland, St. Lucia* QLD 4072*, Australia. E-mail: xing@access.edu.au or h.xing@uq.edu.au*

[2]*Australian Computational Earth Systems Simulator (ACcESS), Major National Research Facility, Sir James Foots Building (47a), The University of Queensland, St Lucia, Brisbane* QLD 4072*, Australia*

Accepted 2007 March 16. Received 2007 March 13; in original form 2006 September 13

SUMMARY

Tidal deformation of the Earth is normally calculated using the analytical solution with some simplified assumptions, such as the Earth is a perfect sphere of continuous media. This paper proposes an alternative way, in which the Earth crust is discontinuous along its boundaries, to calculate the tidal deformation using a finite element method. An in-house finite element code is firstly introduced in brief and then extended here to calculate the tidal deformation. The tidal deformation of the Earth due to the Moon was calculated for an geophysical earth model with the discontinuous outer layer and compared with the continuous case. The preliminary results indicate that the discontinuity could have different effects on the tidal deformation in the local zone around the fault, but almost no effects on both the locations far from the fault and the global deformation amplitude of the Earth. The localized deformation amplitude seems to depend much on the relative orientation between the fault strike direction and the loading direction (i.e. the location of the Moon) and the physical property of the fault.

Key words: crustal deformation, deformation, finite-element methods, gravity, tides.

1 INTRODUCTION

Tidal deformation/stress of the Earth results from the combination of the gravitational forces mostly from the Sun and the Moon and the inertial acceleration of the centre of mass of our planet in its revolution around the Sun and around the centre of mass of the Earth–Moon system. In a Keplerian rotation, this acceleration is constant inside the Earth body and one can demonstrate that the gravitational attraction and the inertial acceleration cancel each other at the mass centre of the Earth. The deformation of the Earth due to extraterrestrial forces is an important topic in geophysics, which is highly required for research on Earth deformation, earthquake triggering mechanisms, high precision work using GPS as well as tidal heating, etc. (e.g. Ross & Schubert 1987). In earlier time, it was mainly due to lack of high computing power that we had to resort to simple models. The geophysical earth models have advanced from the simplest Gutenberg–Bullen Model to the more complex (yet coarse) Preliminary Reference Earth Model (PREM) until recently when a few 3-D models have been introduced. However, in the existing computations of the tidal deformation, only 1-D models are used. They mostly share the common nature of being purely elastic, isotropic, homogeneous, continuous and spherically symmetrically layered (e.g. Melchior 1978). In recent models, inelasticity of the Earth mantle and discontinuities inside the Earth are introduced with specific conditions, but the discontinuous outer layer of the Earth is not modelled (Dehant 1987; Dehant *et al.* 1999; Mathews *et al.* 2002). So, measuring purely by the complexity of approach, computation of earth tides has fallen behind the geophysical earth model development.

The existing knowledge about the tidal deformation maybe deviates little from the reality when dealing with the deformation of deeper structure of the Earth. But when we are investigating phenomena occurred in the lithosphere, which is mostly relevant to our life, we cannot consider the crust as continuous media. In fact, the Earth is not a homogeneously continuous media due to multiple plates, thousands of faults, etc. To date, no results on comprehensive or qualitative estimation of the global distribution of the tidal deformation in the crust and evaluation of the related effects considering the above factors are available. The current understanding of crustal deformation is far from being able to solve the complexity of tectonic plate movement, earthquakes, etc. Sooner or later, discontinuous Earth modelling has to be applied. The existing calculations of tidal deformation are based on Love Numbers, which are related to the rheological properties of the Earth (e.g. Munk & MacDonald 1960). The Love Numbers are given for continuous media depending on the earth models employed. Since the lithosphere is discontinuous, the actual Love Numbers may be measurably different from the results using continuous assumption at the surface. Also, we don't know how much the discontinuity affects the tidal deformation.

The finite element methods (FEM) are now widely applied to certain science and engineering problems and provide a way to simulate the discontinuity-related system changes. Some researchers

have applied it to the analysis of the ground movement and earthquakes (e.g. Bird 1978; Golke *et al.* 1996; Huang *et al.* 1997; Bao & Bielak 1998; Cai *et al.* 2000; Jimenez-Munt *et al.* 2001; Xing & Makinouchi 2002a; Xing *et al.* 2004b, 2006; Xing & Mora 2006). Among them, Xing *et al.* developed a robust and efficient finite element model capable of simulating the frictional behaviour of rocks and faulting, displacement/velocity and stress evolution of an interacting fault system in both the experimental and practical site scale (e.g. Xing & Makinouchi 2002a,b, 2003; Xing *et al.* 2004b, 2006; Xing & Mora 2006). Thus, with the improvement of hardware and software, it becomes possible to calculate the tidal deformation of a discontinuous Earth. The above model developed by Xing *et al.* (e.g. Xing & Makinouchi 2002a,b, 2003; Xing *et al.* 2004b, 2006; Xing & Mora 2006) is extended and applied here to the analysis of the tidal deformation of the entire Earth using the parallel supercomputing. This paper focuses on the investigation of the effect of discontinuous media (i.e. the fault/plate boundary) on the tidal deformation, including the comparison with results from a continuous earth model.

2 FEM GOVERNING ALGORITHMS AND EQUATIONS

A three-dimension R-minimum strategy based finite-element computational algorithm for modelling frictional contact behaviours between multiple deformable bodies with the arbitrarily shaped contact element strategy was proposed and developed by Xing *et al.* and successfully applied in a wide field, the part of which related with the crustal dynamics is briefly summarized as follows.

2.1 Finite-element formulation

The updated Lagrangian rate formulation is employed to describe the non-linear contact problem. The rate type equilibrium equation and the boundary at the current configuration are equivalently expressed by a principle of virtual velocity of the form (e.g. Xing *et al.* 1998; Xing & Makinouchi 2000, 2003)

$$\int_V \left(\tau_{ij}^{\circ} - D_{ik}\sigma_{kj} + \sigma_{ik}L_{jk} - \sigma_{ik}D_{kj}\right)\delta L_{ij}dV = \int_{S_F} \dot{F}_i \delta v_i dS + \int_{S_{c1}} \dot{f}_i^1 \delta v_i dS + \int_{S_{c2}} \dot{f}_i^2 \delta v_i dS \quad (1)$$

where V and S denote, respectively, the domains occupied by the total deformable body B and its boundary at time t; S_F is a part of the boundary of S on which the rate of traction $\dot{F}_i$ is prescribed; $\boldsymbol{v}$ is the virtual velocity field which satisfies the condition $\delta\boldsymbol{v} = 0$ on the velocity boundary; τ_{ij}° is the Jaumann rate of Cauchy stress; $\boldsymbol{L}$ is the velocity gradient tensor, $\boldsymbol{L} = \partial\boldsymbol{v}/\partial\boldsymbol{x}$; $\boldsymbol{D}$ and $\boldsymbol{W}$ are the symmetric and antisymmetric parts of $\boldsymbol{L}$, respectively; $\dot{\boldsymbol{f}}^{\alpha}$ is the rate of contact stress on contact interface S_c of the body α and calculated as follows.

2.2 Frictional contact

A unified constitutive equation of frictional contact has been proposed and implemented in the code by Xing *et al.* (2006). It is summarized as follows. The penalty parameter method is chosen to satisfy the normal impenetrability condition when contact occurs, thus the normal contact stress f_n can be calculated as

$$f_n = \boldsymbol{f}\cdot\boldsymbol{n} = E_n g_n \quad (\neq 0 \text{ only for } g_n < 0), \quad (2)$$

here g_n is the penetration (gap) in the normal direction; E_n is the penalty parameter to penalize the penetration (gap) in the normal direction, we take $E_n = \wp\frac{KA^2}{V}$, where A and V are, respectively, the contact surface area and the volume of a solid element (a eight-node hexahedron element is used here); K is the bulk modulus; $\wp$ is the prescribed parameter.

As for the frictional slip, an increment decomposition of the sticking and the slipping is assumed. A standard Coulomb friction model is applied in an analogous way to the flow plasticity rule to govern the slipping behaviour. Thus, the frictional stress can be described as follows (Xing & Makinouchi 2002a, 2003; Xing *et al.* 2006) (a variable with tilde (~) denotes a relative component between slave and master bodies, and $l, m = 1, 2; i, j, k = 1, 2, 3$ in this paper if not otherwise specified):

$$f_l = E_t\tilde{u}_l^e = E_t\sum\Delta\tilde{u}_l^e, \quad df_l = E_t d\tilde{u}_l \quad \text{(in the sticking state)} \quad (3)$$

$$df_l = \frac{\overline{F}E_t}{\sqrt{f_m^e f_m^e}}\left(\delta_{lm} - \eta_l\eta_m\right)d\tilde{u}_m + \eta_l\mu\left(df_n + \frac{\partial\mu}{\partial f_n}df_n\right) + \eta_l f_n\left(\frac{\partial\mu}{\partial\dot{\tilde{u}}_{eq}^{sl}}d\dot{\tilde{u}}_{eq}^{sl} + \frac{\partial\mu}{\partial\varphi}d\varphi\right) \quad \text{(in the slipping state).} \quad (4)$$

Here μ is the friction coefficient, it may depend on the normal contact pressure f_n, the equivalent tangential velocity $\dot{\tilde{u}}_{eq}^{sl}$, the state variable φ, that is, $\mu = \mu(\dot{\tilde{u}}_{eq}^{sl}, f_n, \varphi)$. (e.g. Dieterich 1979; Ruina 1983; Scholz 1998).

In summary, from eqs (2)–(4), the contact stress acting on a slave node can be described as (denote $\dot{f}_3 = \dot{f}_n$)

$$\dot{f}_i = G_{ij}\dot{\tilde{u}}_j, \quad (5)$$

where $\boldsymbol{G}$ is the frictional contact matrix for both the stick and the slip state (Xing *et al.* 2006).

2.3 Arbitrarily shaped contact element strategy

A node-to-point contact element strategy was proposed to handle the frictional contact problems between deformable bodies (Xing *et al.* 1998; Xing & Makinouchi 2000, 2002a,b) and is briefly introduced here. Assume a slave node s has contacted with point c on a surface element (master segment) E', and the surface element E' consists of γ nodes ($\gamma = 4$ in this paper if without special notation), thus the term related with contact in eq. (1) can be described as [$\alpha = 1, (\gamma + 1), \beta = 1, (\gamma + 1)$]

$$\dot{f}_i(\delta u_{si} - \delta u_{ci}) = \delta\dot{u}_{sci\beta}\left[\overline{K}_{fik}\right]_{\beta\alpha}\dot{u}_{sck\alpha}, \quad (6)$$

where

$$\left[\overline{K}_{fik}\right]_{\beta\alpha} = R_\beta\boldsymbol{e_i}\cdot\{G_{hk}R_\alpha\boldsymbol{e_h} + \left(H_{jm}\hat{\boldsymbol{e}}_{\boldsymbol{j}}\left(\left(\overline{C}_{ll}R_{\alpha,m} - \overline{C}_{ml}R_{\alpha,l}\right)\boldsymbol{e_k}\cdot\tilde{\boldsymbol{x}}\right.\right. + R_\alpha\left(\overline{C}_{ll}\hat{\boldsymbol{e}}_{\boldsymbol{m}} - \overline{C}_{ml}\hat{\boldsymbol{e}}_{\boldsymbol{l}}\right)\cdot\boldsymbol{e_k})\}$$
$$(h = 1, 2, 3, l \neq m \text{ and no sumon } l), \quad (7)$$

here $\overline{C}_{ml} = C_{ml} - g_n\boldsymbol{n}\cdot\hat{\boldsymbol{e}}_{\boldsymbol{m},\boldsymbol{l}}$, $C_{ml} = \hat{\boldsymbol{e}}_{\boldsymbol{m}}\cdot\hat{\boldsymbol{e}}_{\boldsymbol{l}}$, $\wp = \overline{C}_{11}\overline{C}_{22} - \overline{C}_{12}\overline{C}_{21}$, $\tilde{\boldsymbol{x}} = \boldsymbol{x_s} - \boldsymbol{x_c}$, $E_{ijm} = \hat{\boldsymbol{e}}_{\boldsymbol{i},\boldsymbol{m}}\cdot\hat{\boldsymbol{e}}_{\boldsymbol{j}}$, $H_{jm} = \hat{f}_i E_{ijm}/\wp$, $R = [\,1\ -N_1\ -N_2\ \ldots\ -N_\gamma\,]^T$, $N_p(p = 1, \gamma)$ is the shape function value of the point c on the surface element E', $\hat{\boldsymbol{e}}_{\boldsymbol{i}}$ and $\boldsymbol{e_i}$ are, respectively, the base vectors of the local natural and the local Cartesian coordinate systems on the master segment.

2.4 Time integration algorithm

The time integration method is one of key issues to formulate a nonlinear FEM. It is well known that the fully implicit method often suffers from bad convergence for the non-linear problems, such as due to changes of contact and friction states. In order to avoid this, we employ an explicit time integration procedure as follows. It is assumed that under a sufficiently small time increment all rates in eq. (1) can be considered constant within the increment from t to $t + \Delta t$ as long as there are no drastic changes of state takes place. The R-minimum method is used to limit the step size in order to avoid such a drastic change in state within an incremental step (e.g. Xing & Makinouchi 2002b).

Thus all the rate quantities used to derive eq. (1) are simply replaced by incremental quantities as

$$\Delta \boldsymbol{u} = \boldsymbol{v}\Delta t = \dot{\boldsymbol{u}}\Delta t, \tag{8}$$

$$\Delta \boldsymbol{\tau} = \mathring{\boldsymbol{\tau}}\,\Delta t. \tag{9}$$

Finally, in combination with the above equations, eq. (1) can be rewritten as

$$(\boldsymbol{K} + \boldsymbol{K}_f)\Delta \boldsymbol{u} = \Delta \boldsymbol{F} + \Delta \boldsymbol{F}_f, \tag{10}$$

here $\boldsymbol{K}$ and $\Delta \boldsymbol{F}$ are, respectively, the stiffness matrices and force increment terms corresponding to the various time integration algorithms; $\boldsymbol{K}_f$ and $\Delta \boldsymbol{F}_f$ are the stiffness matrices and the force increments of all the contact elements among the contact pairs. As for the details on how to solve the above equations for large scale problems, please refer to Xing *et al.* (1998) and Xing & Makinouchi (2002a).

A 3-D finite element software PANDAS has been developed using the above algorithm and tested with various applications in mechanical/materials engineering (e.g. Xing *et al.* 1998, 2004a; Xing & Makinouchi 2001) and geo-science and engineering, such as the so-called sandwich fault model (Xing & Makinouchi 2002c), single fault bend model including both the interplate (Xing & Makinouchi 2003) and the intraplate cases (Xing *et al.* 2003, 2004b)), multiple fault bends model (Xing *et al.* 2006), the practical interacting fault systems (such as the South Australia fault system) (Xing & Mora 2006). It will be extended here to simulate the tidal deformation.

3 TIDAL DEFORMATION FORMALISM

According to Newton's law of universal gravitation, the force of gravity between two point masses, m_1 and m_2, separated by a distance r is attractive and of magnitude

$$F = G\frac{m_1 m_2}{r^2}, \tag{11}$$

where G is the Newtonian constant of gravitation, $G = 6.67 \times 10^{-11}$ N m^2 kg^{-2} (NIST 2002).

Since the purpose of this paper is to assess the effect of discontinuous outer layer (crust) on the tidal deformation, and the Moon–Earth gravitational forces are twice those of the Sun–Earth, only the interaction between the Earth and the Moon is examined while the force of the Sun is omitted. The tidal deformation of the Earth results from the combination of the gravitational forces between the Earth and the Moon and centrifugal force in the Earth. As deduced by Newton in his famous Mathematical Principles of Natural Philosophy (Newton 1729), the gravitational force between the Moon with mass m and an arbitrary mass point P_i within the Earth with mass m_i is equivalent to the force exerted on the mass point $m_i$by a point mass m positioned at the centre of the Moon (Fig. 1). Therefore, the intensity F_i of the gravitational force between the Moon with mass m and an arbitrary mass point P_i can be written as,

$$F_i = G\frac{m_i m}{r_i^2}, \tag{12}$$

where the force acts towards the Moon centre as shown on Fig. 1; $m = 7.3483 \times 10^{22}$ kg (NASA 2007) and r_i is the distance between the centre of the Moon and point P_i.

Since gravitational attraction is a function of the distance between two separate masses (as in eqs 11 and 12), the lunar attraction force on the Earth is not uniform. Some parts of the Earth are more strongly attracted to the Moon than the others. Tidal deformation increases as an astronomical object moves closer to the body it orbits. As described in the Introduction section, in a Keplerian rotation, one can demonstrate that the gravitational attraction and the inertial acceleration cancel each other at the mass centre of the Earth. We can thus compute the tidal forces as the difference between the gravitational attraction of a celestial body (i.e. the Moon) at any location inside the Earth and the gravitational attraction at the centre of the Earth. Therefore, the tidal force $\boldsymbol{F}_{Ti}$ on the point P_i, which governs the tidal deformation, can be described as,

$$\boldsymbol{F}_{Ti} = \boldsymbol{F}_i - \boldsymbol{F}_{0i}, \tag{13}$$

where $\boldsymbol{F}_{0i}$ is the reference attraction force on the point P_i acting at the centre point P of the Earth; from eq. (11), its magnitude can be described as

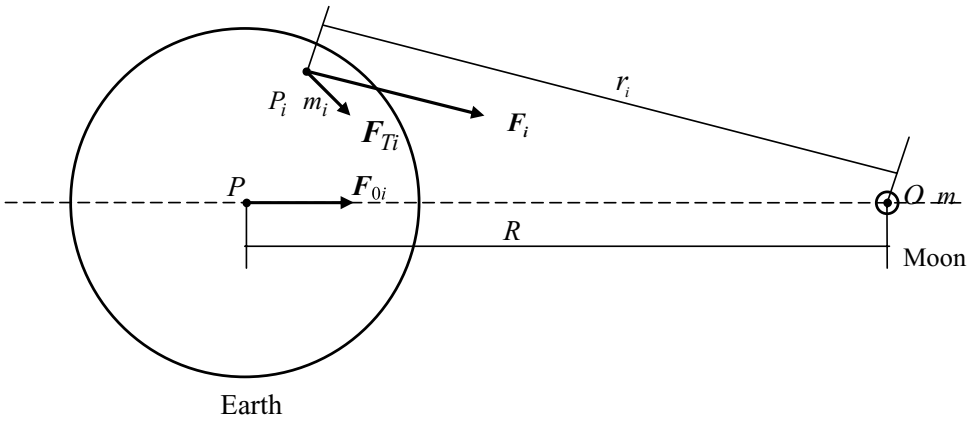

Figure 1. The related forces between the Moon and the Earth. The tidal force $\boldsymbol{F}_{Ti}$ at any location P_i inside the Earth is computed as the difference between the gravitational attraction force $\boldsymbol{F}_i$ of a celestial body (i.e. the Moon) at the point P_i and the gravitational attraction force$\boldsymbol{F}_{0i}$ at the centre of the Earth.

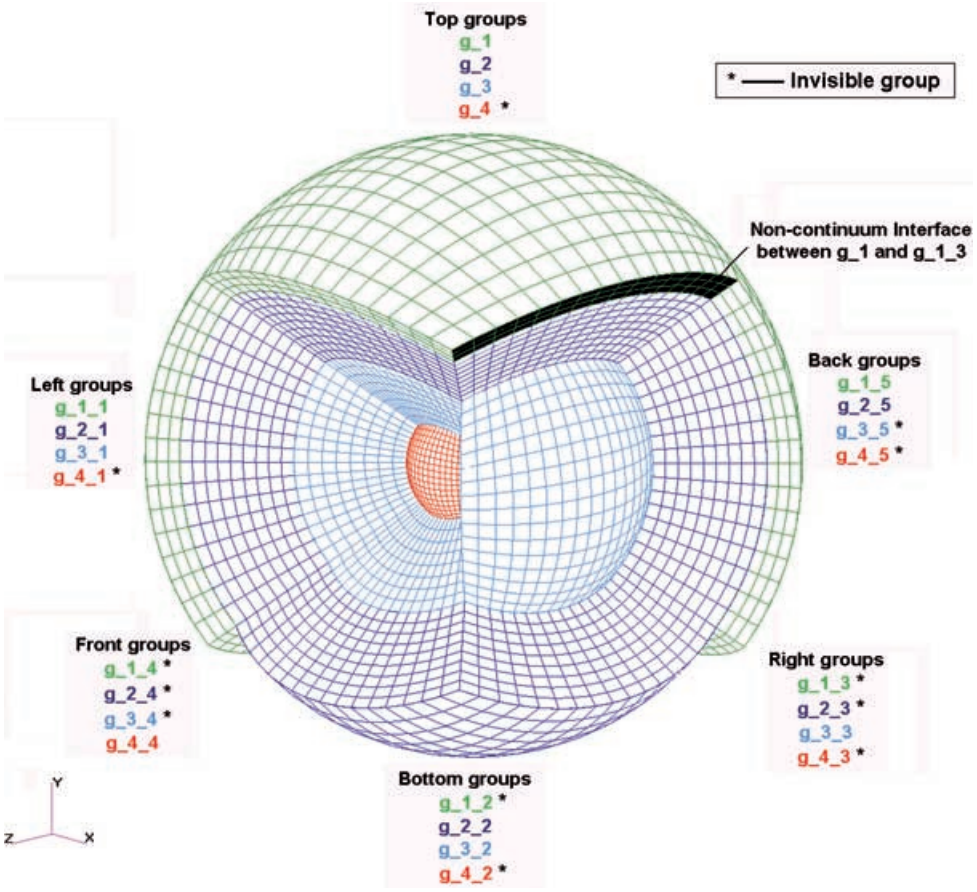

Figure 2. The entire geophysical earth model to be analysed. It is composed of four layers (from the inside to the outside): the inner core, the outer core, the mantle and most outer layer (crust), and each layer consists of six groups (see Table 1).

$$F_{0i} = G\frac{m_i m}{R^2}, \tag{14}$$

where R is the distance between the central points P and O of the Earth and the Moon; see Fig. 1.

The above eqs (12)–(14) are implemented to our finite element code as introduced above, which is similar to what was done for the hydraulic loading case by Xing & Makinouchi (2001).

Table 1. Definition of the different groups in the mesh generation using MSC Patran software.

	Top	Left	Bottom	Right	Front	Back
Inner core	g_4	g_4_1	g_4_2	g_4_3	g_4_4	g_4_5
Outer core	g_3	g_3_1	g_3_2	g_3_3	g_3_4	g_3_5
Mantle	g_2	g_2_1	g_2_2	g_2_3	g_2_4	g_2_5
Out layer	g_1	g_1_1	g_1_2	g_1_3	g_1_4	g_1_5

4 COMPUTATION RESULTS

4.1 The whole earth modelling for tidal deformation computation

Because the purpose of this paper is to assess the effect of discontinuity on tidal deformation, only a four-layered geophysical earth model is used, which is composed of the inner core, the outer core, the mantle and the outer layer (including the crust and the transition zone), Fig. 2. The property of each layer is taken from the PREM model (Dziewonski & Anderson 1981). The software MSC Patran (Patran 2004) is used for the mesh generation. For convenience, the group technique of Patran is applied here. Each layer of the above whole earth model consists of six groups, thus 24 groups are generated in the whole earth model (Table 1 and Fig. 2), the model construction and mesh generation are much more simplified. The whole earth is discretized into 44 602 nodes and 43 008 hexahedron elements for the continuous case, Fig. 2. For simplicity, the same material parameters in each layer (but varying amongst the different layers) are used here, and all the materials are assumed to be non-compressively elastic. Table 2 lists the material parameters used.

4.2 Tidal deformation

To investigate the effects of the seismic faults/plate boundary (i.e. the discontinuous outer layer of the Earth) on the tidal deformation, the following cases were investigated, where no tension force is permitted along the normal direction of the fault. All the following results are shown in the normal scale except those specially noted using the exaggerated scale.

4.2.1 The continuous geophysical earth model

The continuous geophysical earth model (i.e. no faulting) is initially computed with the Moon positioned at the X axis, that is, the (1 0 0) direction, see Figs 2 and 3. Both the total displacement and its

Table 2. Physical properties of the different layers as used in the analysis (all calculated from Dziewonski & Anderson 1981).

	Radius range (km)	Density (10^3 kg m^{-3})	Bulk module (MPa)	Poisson's ratio
Inner core	0–1300	13.01009	1405 300	0.4900
Outer core	1300–3500	11.29298	1015 800	0.4800
Mantle	3500–5730	5.00299	476 600	0.2898
Out layer	5730–6400	3.48951	163 000	0.2952

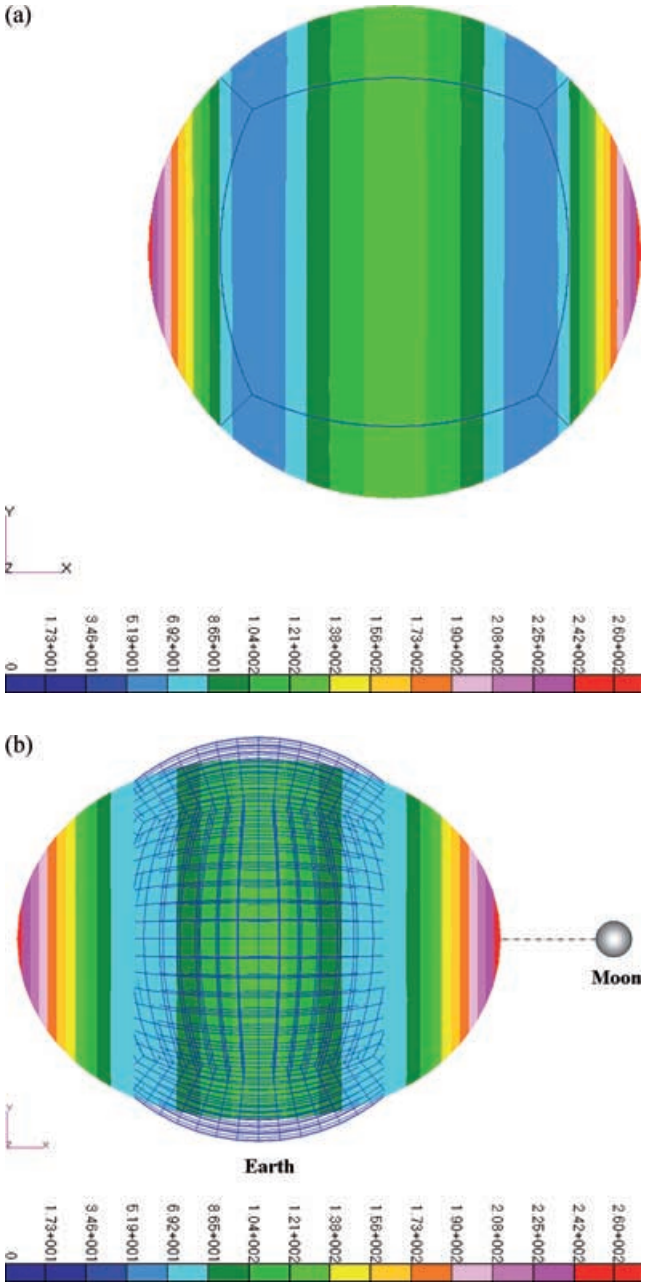

Figure 3. The total displacement distribution for the continuous geophysical earth model when the Moon is located at the positive direction of the *X* axis, that is, the (1 0 0) direction (unit: mm) (a) at the outside surface in the *XY* plane; (b) at the outside surface in the *XY* plane with the exaggerated scale; (c) at the outside surface in the *XYZ* space with the exaggerated scale and (d) at the different layers in the *XYZ* space. The blue grids in (b) and (c) represent a part of the original configuration of the Earth before tidal deformation.

Figure 3 (*Continued.*)

components are distributed smoothly and continuously as indicated by Figs 3 and 4, respectively. Also, comparing with the calculation results of displacement with the analytical solution as described in Yin (2006), both distribute continuously and smoothly (i.e. neither has singular points/zones appearing for the displacement distribution); the maximum displacement occurs along the central line of the Earth–Moon in both cases; and their values reasonably agree with each other. For the analytical one, the maximum displacement

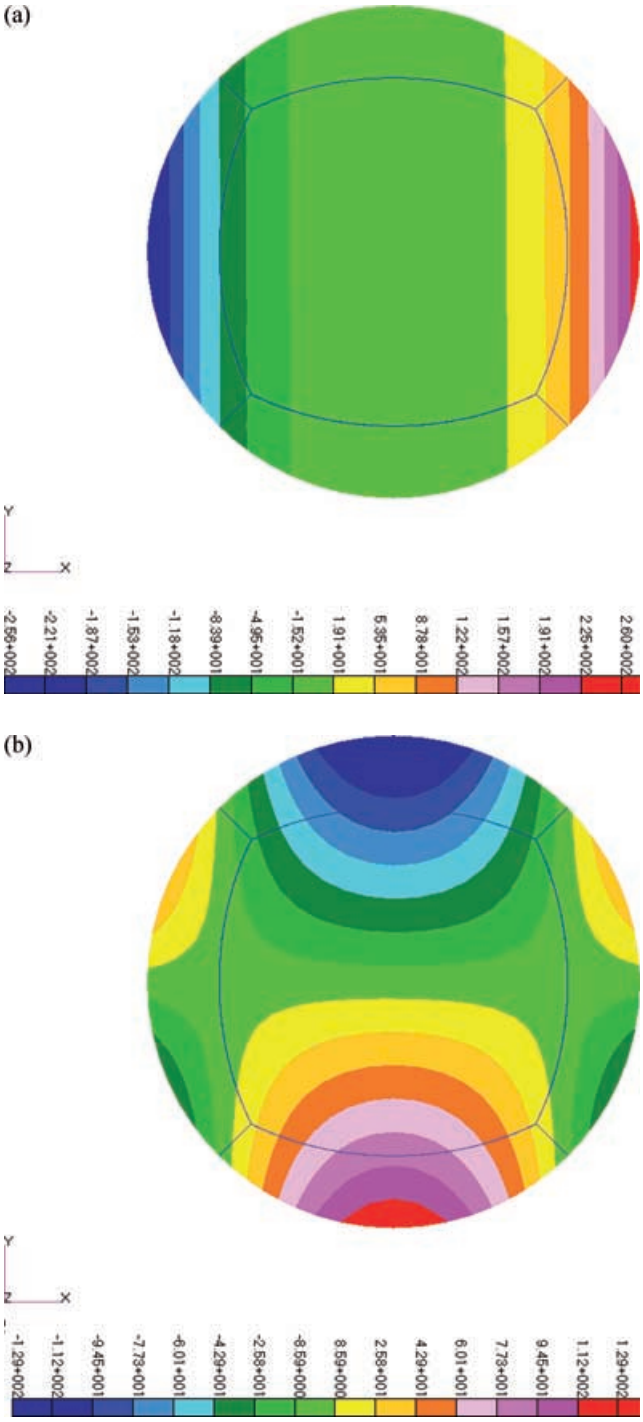

Figure 4. The displacement component distribution for the continuous geophysical earth model in the *XY* plane when the Moon is located at the positive direction of the *X*-axis, that is, the (1 0 0) direction (unit: mm): (a) the component along the *X*-axis and (b) the component along the *Y*-axis or the *Z*-axis

value is 254 mm and they are the same at both sides; for the FEM case, the maximum displacement values are different at the both sides, they are 260 mm at the side closer to the Moon and 256 mm at the other side.

4.2.2 The discontinuous geophysical earth model

An idealized case, that is, a simple representation of a fault at the outer layer of the four layered earth model subjected to the Moon–Earth gravitational force, is applied as follows to investigate the effect of discontinuous media on the tidal deformation. Assume that a fault (i.e. a discontinuous seismogenic interface) exists in the outer layer between the groups g_1 and g_1_3 as shown on Figs 2 and 5(a, b and e), where g_1 and g_1_3 groups are according to Table 1. Both the tidal force subjected to the Earth (eq. (13)) and the relative orientation between the fault strike and the tidal force loading direction vary with the change in the location of the Moon. The following two cases are investigated here: the Moon positions at the positive directions of the *X* and the *Z* axis, that is, the (1 0 0) and the (0 0 1) direction. For simplicity, we denote them as the cases A and B, respectively. Figs 5(a–h) and 6(a–e) show the

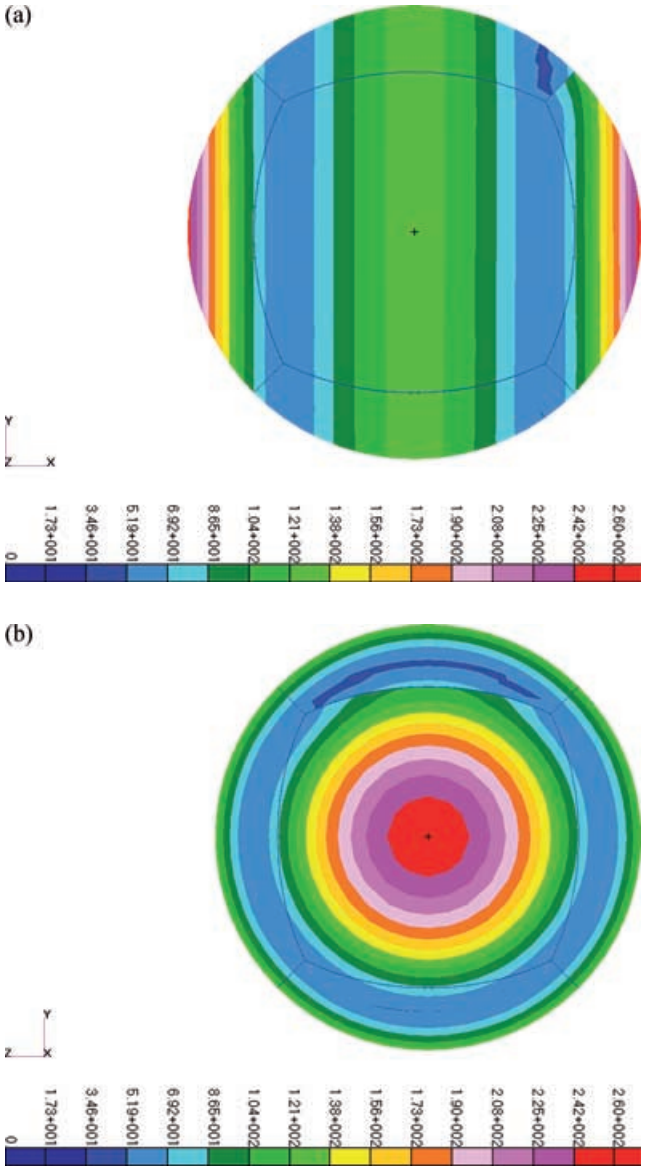

Figure 5. A fault is located between the group g_1 and g_1_3 at the crust layer. When the Moon is located at the positive direction of the *X* axis, that is, the (1 0 0) direction, it is denoted as the case A. The total displacement distribution viewed at the different spaces (unit: mm) : (a) in the *XY* plane; (b) in the *YZ* plane; (c) in the *XZ* plane; (d) in the *XZ* plane after the removal of the group g_1 and (e) in the *XYZ* space. The individual displacement component distribution for the case A viewed at the different spaces: the component along the *Y*-axis viewed in the *XY* plane (f); the component along the *Z*-axis viewed (g) in the *ZY* plane and (h) in the *YZ* plane.

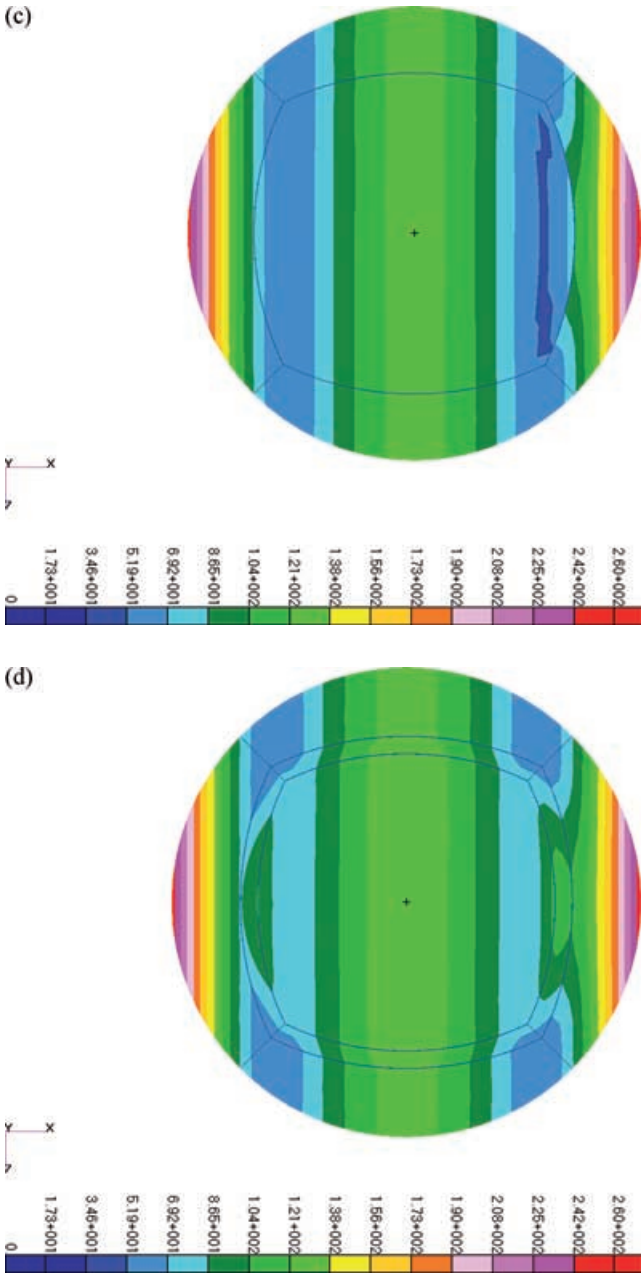

Figure 5 (*Continued.*)

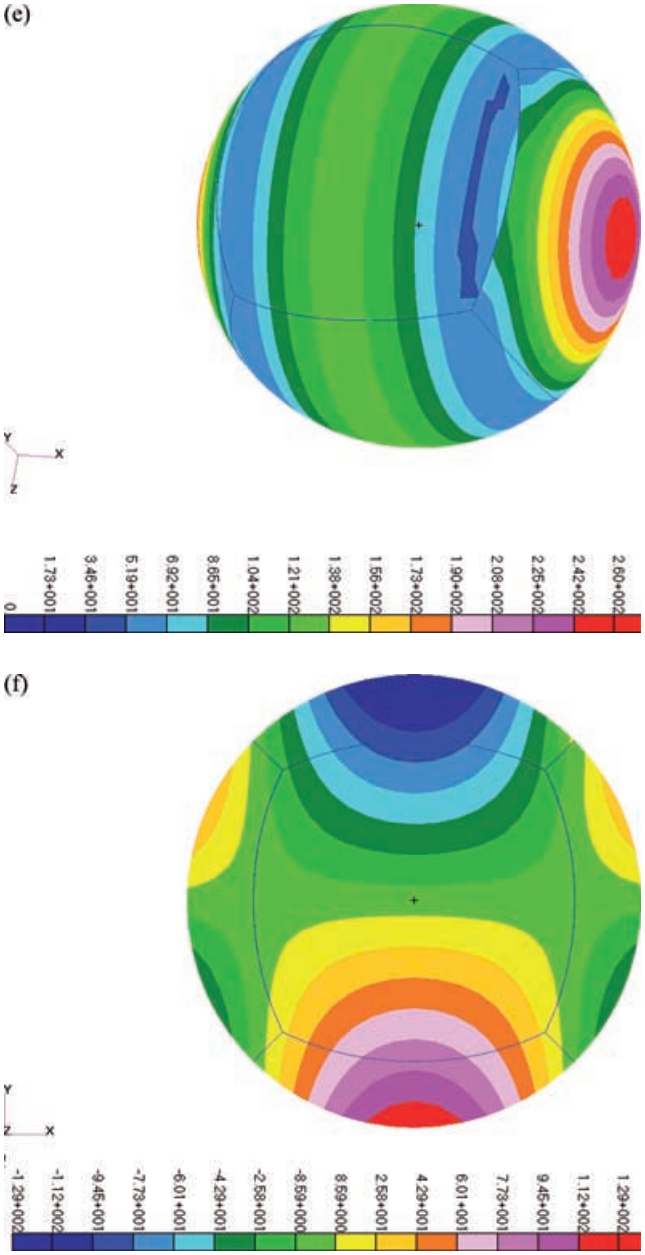

Figure 5 (*Continued.*)

results of the displacement distribution calculations for the cases A and B ($\wp = 0$), respectively. Comparing with the continuous model (as shown on Figs 3 and 4), the fault appears to affect the deformation in the localized zone around the fault for both the total displacement (as shown on Figs 5a–e and 6a–c) and its components distribution (as shown on Figs 5f–h and 6d and e). The fault (i.e. the discontinuous outer layer) destroys the continuity of the deformation (i.e. the displacement and its components distribution), which makes it different from the continuous geophysical earth model. However, the fault does not seem to affect the other part of the Earth farther from the fault (as shown on Figs 5a–e and 6a–c) and its components distribution (as shown on Figs 5f–h and 6d and e), as well as the maximum deformation amplitude of the Earth for the current cases studied as shown on Figs 3(b), 5(e) and 6(b).

For the above calculations, the parameter E_n input for the fault does not appear to affect the calculated results for the case A, however the situation reverses for the case B. Because the relative locations of the Moon with respect to the fault for the cases A and B are different, this makes the loading force directions around the fault different—it is in the tension state for the case A, but in the compression state for the case B. For the case B, if the penalty parameter E_n along the fault is taken big enough (such as $\wp = 100$), there is no difference found for the calculated results from the above continuous model as shown on Figs 3(b) and 7. However, when the parameter is taken to be small (such as $\wp = 0.001$), the discontinuous distribution of the calculated results around the fault (i.e. the displacement and its components) becomes obvious; and the smaller the parameter is, the more obvious the difference from the continuous model is (as shown on Figs 6a–e and 7). Here, Figs. 6(a)–(e) show the results when $\wp = 0$, which correspond to the very weak materials existing around the fault or a gap existing along the fault. All the above also demonstrate that the amplitudes of effect from the fault are quite

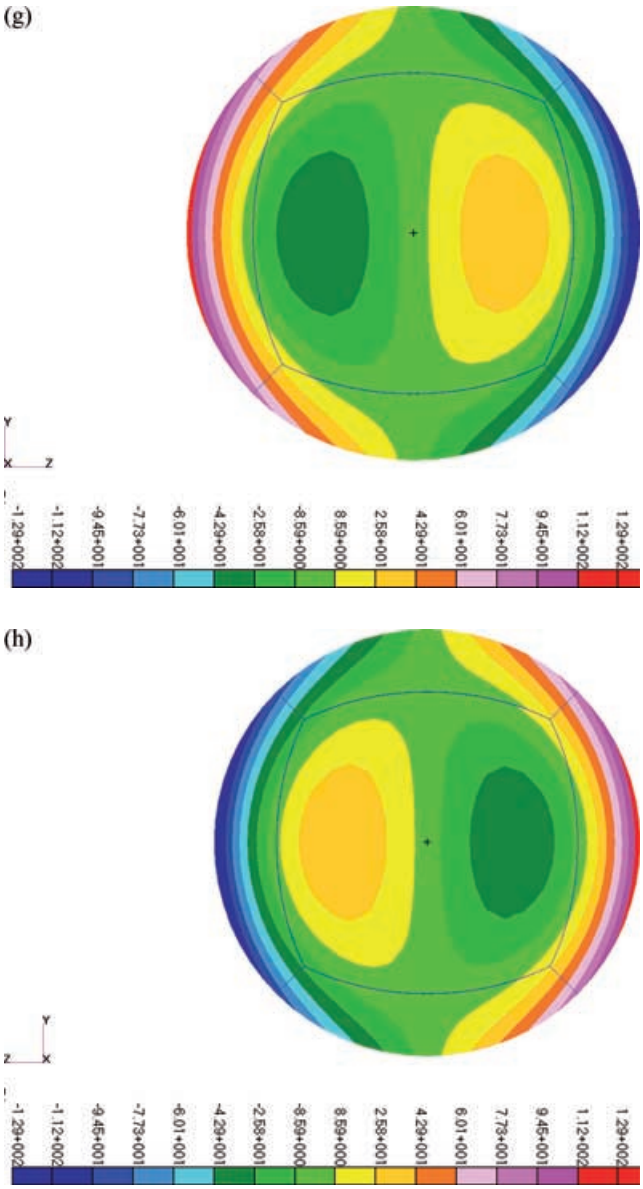

Figure 5 (*Continued.*)

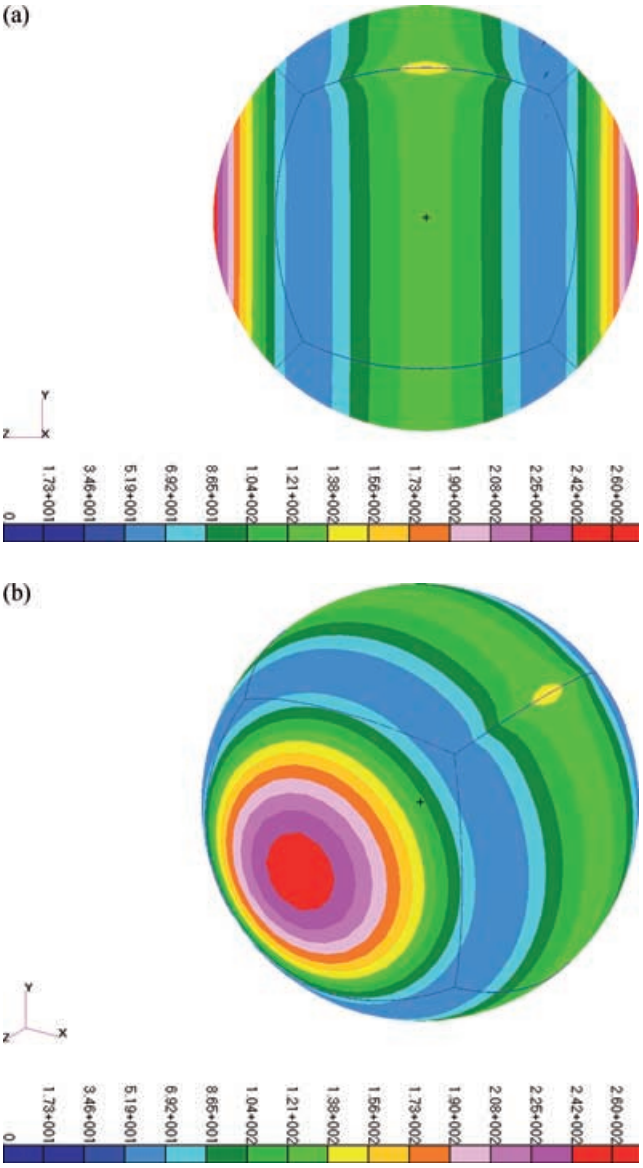

Figure 6. A fault is located between the group g_1 and g_1_3 at the crust layer. When the Moon is located at the positive direction of the *Z*-axis, that is, the (0 0 1) direction, it is denoted as the case B. The total displacement distribution (unit: mm) viewed at the following different space (with $\wp$ = 0) (a) in the *YZ* plane; (b) in the *XYZ* space; (c) in the *XYZ* space after the removal of the groups g_1 and g_2. The individual displacement component distribution for the case B viewed at the different space: the component along the *X*-axis viewed (d) in the *ZX* plane and (e) in the *XZ* plane.

different, depending on the relative orientation between the fault strike direction and the loading direction (i.e. the location of the Moon) for the cases A and B as shown on Figs 5(a)–(h) and 6(a)–(e), as well as on the fault properties (fault strike direction, fault strength and state, for example, for the case B, as shown on Figs 6(a)–(c) and 7 for $\wp = 0$ and 100, respectively).

5 DISCUSSION AND CONCLUSIONS

The FEM has been applied to calculate the tidal deformation of the Earth as an alternative way to currently used analytical approaches which require the specified assumptions. The tidal deformation of the entire Earth with the discontinuous outer layer has been investigated and compared with the continuous model. The preliminary results demonstrate that the discontinuity (fault/plate boundary) can affect the tidal deformation in the localized zone around the fault, which cannot be stated for the zone farther from the fault or for the global deformation amplitude of the Earth for the case studied. The localized deformation distribution depends much on the relative orientation between the fault strike direction and the loading direction (i.e. the location of the Moon) as shown on Figs 5 and 6, as well as on the fault properties (i.e. the different $\wp$ values as shown on Figs 6(a)–(e) and 7 for the case B).

Earthquakes are widely regarded as stick-slip instabilities along the complicated plate/fault boundaries due to overwhelming stress concentration (e.g. Brace & Byerlee 1966; Scholz 1998). Scientists have been theorizing about the possibility of tidal triggering of earthquakes for many years, however, tidal triggering has been very difficult to prove. The argument whether there might be a correlation between earthquakes and the tides seems to remain unresolved based on the statistical analysis of specific cases (Rydelek *et al.* 1988; Ambeth & Fairhead 1991; Cochran *et al.* 2004; Stein 2004).

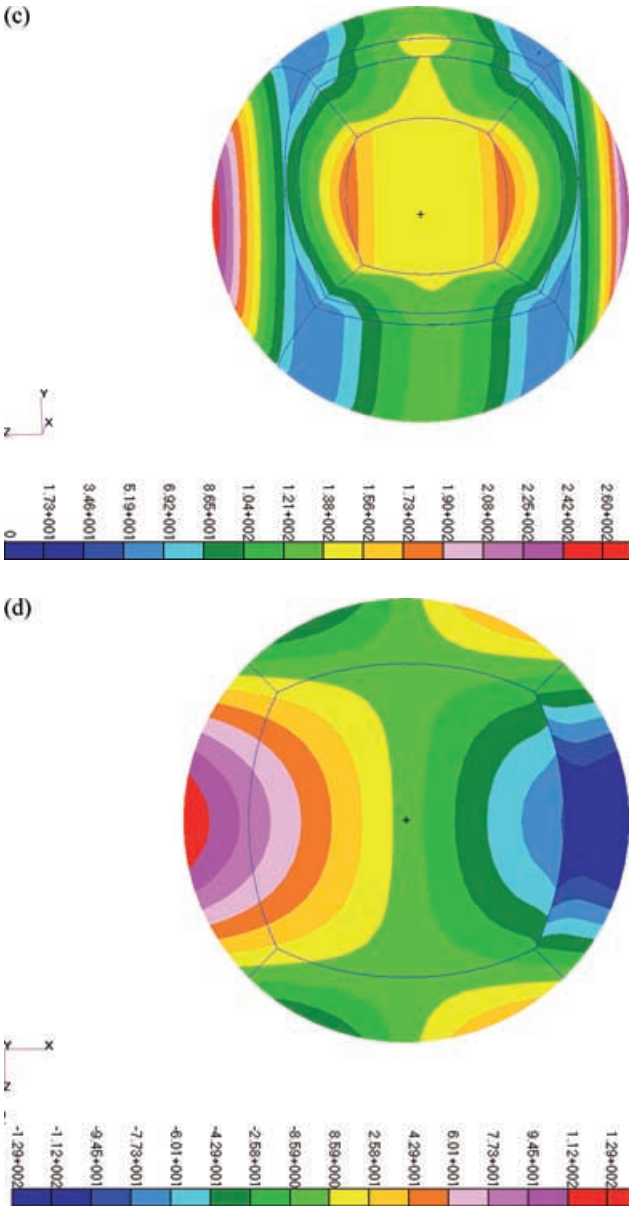

Figure 6 (*Continued.*)

The computations presented here demonstrate that the discontinuity of the most outer layer seems to affect somehow the tidal deformation in the localized zone. The localized deformation distribution seems to depend much on the relative orientation between the fault strike direction and the tidal force loading direction (i.e. the location of the Moon), thus all previous arguments involving tidal deformation may need reinvestigation because the basis for such discussion could be incorrect.

The computed results show that FEM provides a useful approach for studying the Earth's tidal deformation on the global scale involving discontinuity effect. It may be extended for the related research on tidal deformation with the more practical and complex conditions as well as different timescales. In addition, the contribution of tidal deformation to the instability of focal media depends on frictional and other material properties—by incorporating their updated values with other rheological data as those become available, and by varying these properties we hope to discover a more decisive relationship between tidal deformation and earthquakes.

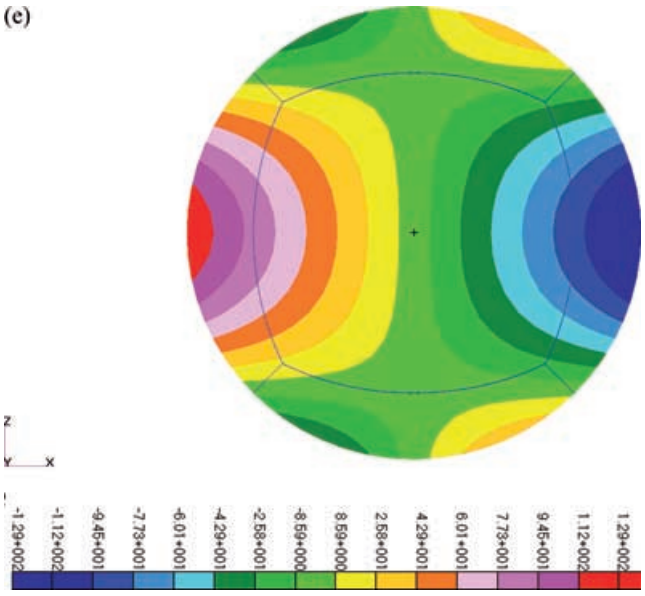

Figure 6 (*Continued.*)

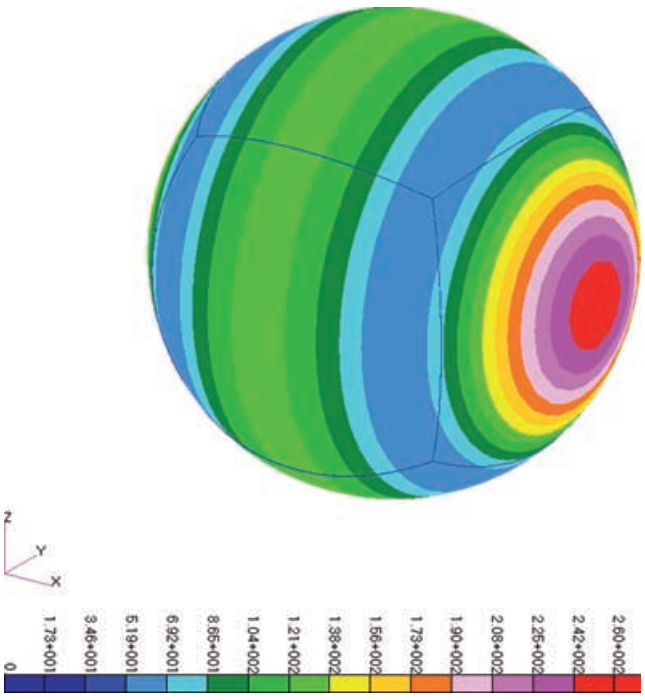

Figure 7. The displacement distribution for the case B with $\wp = 100$ (unit:mm).

ACKNOWLEDGMENTS

Support is gratefully acknowledged by The University of Queensland, Australian Research Council and the Australian Computational Earth Systems Simulator Major National Research Facility (ACcESS MNRF). The authors are grateful to Professor P. Mora and Dr. Y. C. Wang of University of Queensland and Professor X. C. Yin of Geophysics Research Institute of CEA, China for their helpful discussions, to four reviewers for their construction advice/comments that allowed this paper to be improved.

REFERENCES

Ambeh, W.B. & Airhead, J.D., 1991. Regular, deep seismicity beneath Mt. Cameroon volcano: lack of evidence for tidal triggering, *Geophys. J. Int.,* **106,** 287–291.

Bao, H. & Bielak, J., 1998. Large-scale simulation of elastic wave propagation in heterogeneous media on parallel computers, *Comput. Methods Appl. Mech. Engng.,* **152,** 85–102.

Bird, P., 1978. Finite-element modeling of lithosphere deformation: the Zagros collision orogeny, *Tectonophysics,* **50,** 307–336.

Brace, W.F. & Byerlee, J.D., 1966. Stick-slip as a mechanism for earthquakes, *Science,* **153,** 990–992.

Cai, Y., He, T. & Wang, R., 2000. Numerical simulation of dynamic process of the Tangshan earthquake by a new method—LDDA, *PAGEOPH,* **157,** 2083–2104.

Cochran, E.S., Vidale, J.E. & Tanaka S., 2004. Earth tides can trigger shallow thrust fault earthquakes, *Science,* **306,** 1164–1166.

Dehant, V., 1987. Tidal parameters for an inelastic Earth, *Phys. Earth Planet. Int.,* **49,** 97–116.

Dehant, V., Defraigne, P. & Wahr, J., 1999. Tides for a convective Earth, *J. Geophys. Res.,* **104**(B1), 1035–1058.

Dieterich, J.H., 1979. Modelling of rock friction 1. experimental results and constitutive equations, *J. Geophys. Res.,* **84,** 2161–2168.

Dziewonski, A.D. & Anderson, D.L., 1981. Preliminary reference Earth model, *Phys. Earth Planet. Inter.,* **25,** 297–356.

Golke, M., Cloetingh, S. & Coblentz, D., 1996. Finite element modeling of stress patterns along the Mid-Norwegian continental margin, 62°–68° N, *Tectonophysics,* **266,** 33–53.

Huang, S., Sacks, I.S. & Snoke, J.A., 1997. Topographic and Seismic effects of long-term coupling between the subducting and overriding plates beneath Northeast Japan, *Tectonphysics,* **269,** 279–297.

Jimenez-Munt, I., Bird, P. & Fernandez, M., 2001, Thin-shell modeling of neotectonics in the Azores-Gibraltar region, *Geophys. Res. Lett.,* **28,** 1083–1086.

Mathews, P.M., Herring, T.A. & Buffett, B.A., 2002. Modelling of nutation-precession: New nutation series for nonrigid Earth and insights into the Earth's interior. *J. Geophys. Res.,* **107**(B4), ETG3–1–30.

Melchior, P.J., 1978. *The Tides of the Planet Earth*, Pergamon Press, New York.

Munk, W.H. & MacDonald, G.J.F., 1960. The rotation of the Earth: a geophysical discussion. Cambridge University Press, Cambridge, UK.

NASA 2007. Earth's moon, NASA, see http://solarsystem.jpl.nasa.gov/planets/ profile.cfm?Object = Moon

Newton, I., 1729. The mathematical principles of natural philosophy/Translated into English by Andrew Motte. London, printed for B. Motte.

NIST 2002. The NIST Reference on Constants, Units and Uncertainty, http://physics.nist.gov/cuu/Constants/index.html

Patran 2004. MSC.Patran User's Guide and Reference Manuals, MSC Software Corporation, CA, USA. http://www.mscsoftware.com/

Ross, M.N. & Schubert, G., 1987. Tidal heating in an internal ocean model of Europa, *Nature,* **325,** 133–134.

Ruina, A.L., 1983. Slip instability and state variable friction laws, *J. Geophys. Res.,* **88,** 10 359–10 370.

Rydelek, P.A., Davis, P.M. & Koyanagi, R., 1988. Tidal triggering of earthquake swarms at Kilauea volcano, Hawaii, *J. Geophys. Res.,* **93,** 4401–4411.

Scholz, C.H., 1998. Earthquakes and friction laws, *Nature,* **391,** 37–42.

Stein, R., 2004. Tidal triggering caught in the act, *Science,* **305,** 1248–1249.

Suito, H., Iizuka, M. & Hirahara, K., 2002. 3-D Viscoelastic FEM modeling of crustal deformation in northeast Japan, *PAGEOPH,* **159,** 2239–2259.

Xing, H.L., Fujimoto, T., Makinouchi, A. & Nikishkov, G.P., 1998. Static-explicit FE modeling of 3-D large deformation multibody contact problems on parallel computer, in *Simulation of Materials Processing: Theory, Methods and Applications,* 207–212, eds. J. Huetink & F. Baaijens, A.A. Balkema Publishers. Rotterdam/Brookfield.

Xing, H.L. & Makinouchi, A., 2000. A node-to-point contact element strategy and its applications, *RIKEN Review: Focused on High Performance Computing,* **30,** 35–39.

Xing, H.L. & Makinouchi, A., 2001. Numerical analysis and design for tubular hydroforming, *Int. J. Mech. Sci.,* **43,** 1009–1026.

Xing, H.L. & Makinouchi, A., 2002a. Finite-element modeling of multibody contact and its application to active faults, *Concurrency and Computation: Practice and Experience,* **14,** 431–450.

Xing, H.L. & Makinouchi, A., 2002b. Three dimensional finite element modeling of thermomechanical frictional contact between finite deformation bodies using *R*-minimum strategy, *Comput. Meth. Appl. Mech. Eng.,* **191,** 4193–4214.

Xing, H.L. & Makinouchi, A., 2002c. Finite element analysis of sandwich friction experimental model of rocks, *Pure Appl. Geophys.,* **159,** 1985–2009.

Xing, H.L. & Makinouchi, A., 2003. Finite element modeling of frictional instability between deformable rocks, *Int. J. Numer. Anal. Meth. Geomech.,* **27,** 1005–1025.

Xing, H.L., Mora, P. & Makinouchi, A., 2003. Finite element simulation of stress evolution in a frictional contact system, *Lecture Notes in Comput. Sci. LNCS,* **2659,** 798–806.

Xing, H.L., Zhang, K.F. & Wang, Z.R., 2004a. Recent development of mechanics of superplasticity and its applications, *J. Mater. Proc. Tech.,* **151,** 196–202.

Xing, H.L., Mora, P. & Makinouchi, A., 2004b. Finite element analysis of fault bend influence on stick-slip instability along an intra-plate fault, *Pure Appl. Geophys.,* **161,** 2091–2102.

Xing, H.L., Mora, P. & Makinouchi, A., 2006. A unified friction description and its application to the simulation of frictional instability using the finite element method, *Philosophic. Magaz.,* **86,** 3453–3475.

Xing, H.L. & Mora, P., 2006. Construction of an intraplate fault system model of South Australia, and simulation tool for the iSERVO institute seed project, *Pure Appl. Geophys.,* **163,** 2297–2316.

Yin, Can, 2006. Exploring the underlying mechanism of load/unload response ratio theory and its application to earthquake prediction. *PhD thesis*. University of Queensland at St Lucia.